Turkish Journal of Electrical Engineering & Computer Sciences

http://journals.tubitak.gov.tr/elektrik/

Research Article

Turk J Elec Eng & Comp Sci
(2018) 26: 2633 – 2647

doi:10.3906/elk-1801-143

Q-axis current perturbation based active islanding detection for converter interfaced distributed generators

Suman MURUGESAN, Venkatakirthiga MURALI*
Department of Electrical and Electronics Engineering, National Institute of Technology, Tiruchirappalli, India

Received: 16.01.2018 • **Accepted/Published Online:** 19.04.2018 • **Final Version:** 28.09.2018

Abstract: Thanks to the incessant developments in technology towards extracting electric power from renewable energy resources, incorporation of distributed generators has been gaining great importance in recent years. The key expedients for such power generation include reduction in power loss and improvement in the power quality and reliability. In spite of the numerous advantages, it is mandatory to ascertain the island formation and shut down the distributed generators (DGs) during an unplanned islanding. An analyzing technique subsequent to an active islanding detection technique is proposed in this work for faster and accurate detection of island formation. The proposed technique is investigated for various operating conditions, which include source side variations, and validated for various islanding and nonislanding events using the MATLAB R2017b/Simulink platform.

Key words: Microgrid, unintentional islanding, active islanding detection, mean of absolute rate of change of frequency

1. Introduction

Technological developments have made it possible for power engineers and researchers to deploy small generators at the distribution level [1]. The tremendous advantages of such power generation have given a wide scope for researchers to work on the detection of island formation on an unplanned islanding. According to different standards [2–6], it is mandatory to shut down the distributed generators (DGs) on an unplanned islanding owing to uncoordinated protection, inadequate grounding, loss in control over frequency and voltage magnitude, being hazardous to the working personnel since some part of the system remains live, unsynchronized reclosing of the circuit breakers damaging the components in the distribution system including the DG side, etc. The islanding detection time (IDT) of various standards is given in Table 1.

Table 1. Islanding detection time of various standards.

Standard	Q_f	IDT, t (ms)	Standard	Q_f	IDT, t (ms)
IEEE 1547 [6]	1	t < 2000	UL 1741 [5]	≤ 1.8	t < 2000
IEC 62116 [4]	1	t < 2000	VDE 0126-1-1 [3]	2	t < 200
Korean Standard	1	t < 500	IEEE 929-2000 [2]	2.5	t < 2000

Islanding detection strategies (IDSs) are generally categorized into two kinds [7–9]: 1) Remote IDSs and 2) Local IDSs. Communication (with or without a physical link between generating station/substation and

*Correspondence: mvkirthiga@nitt.edu

DGs) based IDSs are termed as remote IDSs [10–12]. Sun and Virgilio have proposed remote islanding detection based on phasor measurement unit [10]. Remote islanding detection based on a communication link between the circuit breaker and inverter is proposed in [11, 12]. Even though the detection time is less, it is unfortunate that they are not suitable for small rated microgrids due to the higher initial investment.

On the other hand, local IDSs are restricted to the point of common coupling (PCC), where the different parameters such as voltage, frequency and total harmonic distortion are monitored at the PCC and assessed to differentiate islanding and nonislanding conditions. Local IDSs [7–9] are subdivided into passive and active types. Passive IDSs detect island formation without any intentional disturbance injected into the system [13–16]. A novel passive IDS based on a duffing oscillator is proposed and implemented in [13]. Impedance magnitude variation based passive IDS is suggested and validated in [13]. An impedance magnitude variation based passive IDS is suggested and validated in [14]. Guha et al. recommended a passive IDS based on voltage ripple in [15]. In [16], the authors have proposed a new passive IDS based on a Helmholtz oscillator. Despite zero power degradation, the higher nondetection zone (NDZ) makes passive IDSs not suitable in most cases. Active IDSs deliberately inject disturbance into the system or add feedback to the control parameters [17–26]. Active IDSs based on reactive power disturbance and rate of change of reactive power are proposed in [18, 22]. Authors in [19, 23] proposed a new active IDS based on voltage magnitude shift on postislanding. An active IDS based on third harmonic injection as a new kind of phase disturbance is suggested in [26].

Active IDSs based on q-axis current disturbance injection are attempted in [17, 20, 21, 24], which do not destabilize the microgrid on postislanding. However, various switching conditions have not been investigated in [17]. Gupta et al. implemented two different frequencies of disturbance signal and proposed analyzing techniques in [20, 24] to distinguish between islanding and nonislanding events, but this technique malidentifies the grid connected operation as island formation [20], when the utility grid operates at a varied frequency by 0.5 Hz than nominal. Moreover, two different frequency injections and intentional delay time make the detection time more (200 ms) for power mismatches between 0% and 16% [24]. The minimum detection time is 200 ms for the technique proposed in [21] due to the intentional delay time of 200 ms. Active IDSs overcome this shortcoming of passive IDSs at the cost of slight degradation in power quality.

In this context, an analyzing technique for renewable energy based DGs like PV and wind is proposed in the present work for faster (less than 160 ms) and accurate islanding detection to overcome the shortcomings based on q-axis disturbance injection. Subsequently an analyzing technique based on mean absolute rate of change of frequency is attempted to detect islanding faster than many IDSs proposed earlier, to accurately distinguish islanding and nonislanding conditions. The proposed analyzing methodology (PAM) has zero NDZ and does not destabilize the system on postislanding conditions. The significance of this proposed methodology is faster islanding detection even on real time varying demands, without using any adaptive threshold. Moreover, the proposed method is found to be robust enough for grid frequency fluctuations as well as the source side fluctuations in solar and wind based DGs. The simulation is done extensively for various grid connected and islanded operating conditions. The detection time is appreciably less than the proposals represented in different standards and also studies in the literature as shown in Table 2.

The proposed methodology is also extended to multiple DGs incorporating solar and wind based inverter DGs. It is clear from Tables 1 and 2 that the detection time is well within various standards and the PAM detects islanding faster than the studies in the literature, respectively.

This paper is organized as follows: the test system for islanding detection in Section 2 follows the

Table 2. Comparison of islanding detection time with the literature.

Reference	Q_f	Detection time (ms)	Reference	Q_f	Detection time (ms)
[25]	0.5	124	[14]	2.5	<350
[16]	0.96	<454	[22]	2.5	356
[15]	1	<300	[23]	2.5	204
[21]	1	>200	Proposed technique	0.5	<125
[13]	1.57	<600		1	<130
[19]	1.77	>200		1.8	<150
[24]	1.8	200		2.5	<160

introduction in Section 1, Section 3 expounds the q-axis current controller for the active IDS followed by significance of current disturbance injection in Section 4. The PAM is elucidated in Section 5, where Section 6 discusses the results for various operating conditions and the paper concludes with Section 7.

2. Test system for islanding detection

A single line diagram of the test system is depicted in Figure 1. A photovoltaic based renewable energy resource is connected to the grid via appropriate converters. The parameters of the test system are tabulated in Section 6. An electronically interfaced DG unit is synchronized with the grid using a phase locked loop. Islanding is simulated by opening the circuit breaker 1 (C.B.1) in Figure 1. The parallel RLC load connected at the PCC is tuned for a resonant frequency of 50 Hz.

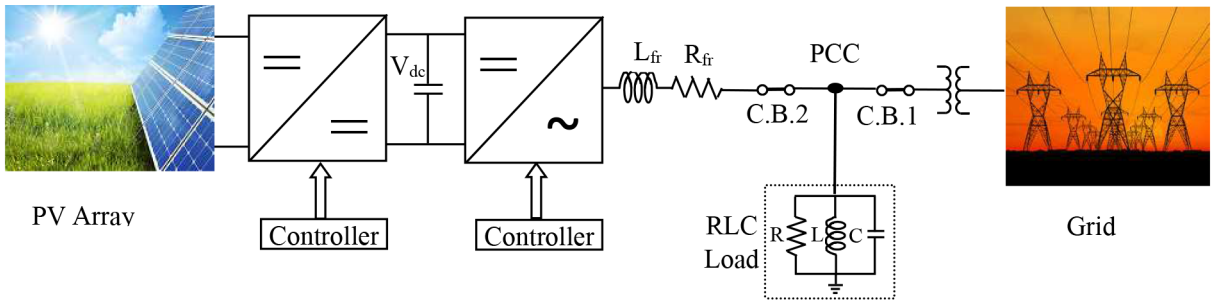

Figure 1. Single line diagram of the test system.

The above test system is also investigated for a wind based permanent magnet synchronous generator unit in this work.

3. Q-axis current controller for the active IDS

The q-axis current controller for the active IDS is explained in this section. The real and reactive powers are controlled by current components of d and q axes, respectively [17, 20], which are expressed as follows:

$$P = \frac{3}{2} v_d i_d \tag{1}$$

$$Q = -\frac{3}{2} v_d i_q \tag{2}$$

The references of i_d and i_q are calculated for the rated d-axis voltage and the rated real and reactive powers, respectively.

For the active IDS, a disturbance signal is injected along with the time tested q-axis current controller. The inverter's output current in terms of dq components is expressed as follows:

$$\begin{bmatrix} i_d \\ i_q \end{bmatrix} = \begin{bmatrix} i_{dref} \\ i_{qref} \end{bmatrix} \tag{3}$$

In general, the electronically interfaced DG unit operates in unity power factor and hence the reference of the q-axis current component i_{qref} is set as zero. Hence the i_q is deduced as follows:

$$i_q = i_{dist} \tag{4}$$

$$i_{dist} = i_{drl}\ sin(\omega_d t) \tag{5}$$

Thus, Eq. 3 is rewritten as follows:

$$\begin{bmatrix} i_d \\ i_q \end{bmatrix} = \begin{bmatrix} i_{dref} \\ i_{qref} + i_{dist} \end{bmatrix}, \tag{6}$$

where i_{drl} – 1% of the rated direct axis current of the DG and ω_d – angular frequency of the current disturbance signal.

The dq0 current components are transformed to abc components by dq0 to abc transformation. The corresponding instantaneous 'a' phase voltage equation for pre- and postislanding conditions is written as follows:

$$v_a = Z_0 i_d sin(\omega_0 t) + Z_1 i_{drl} sin(\omega_1 t + \alpha) + Z_2 i_{drl} sin(\omega_2 t + \beta) \tag{7}$$

$$\omega_0 t = 2\,\pi f_0, \qquad \omega_1 t = 2\,\pi f_1, \qquad \omega_2 t = 2\,\pi f_2, \tag{8}$$

where f_0 - fundamental or nominal frequency, and $f_1 = (f_0 \backsim f_d)$ and $f_2 = (f_0 + f_d)$ represent the difference and sum of the fundamental frequency and disturbance frequency, respectively, where

$$\alpha = -tan^{-1}\left(R\left(\omega_1 C - \frac{1}{\omega_1 L}\right)\right), \qquad \beta = -tan^{-1}\left(R\left(\omega_2 C - \frac{1}{\omega_2 L}\right)\right), \tag{9}$$

$$Z_0 = \frac{1}{\left(\left(\frac{1}{R}\right)^2 + \left(\omega_0 C - \frac{1}{\omega_0 L}\right)^2\right)^{\frac{1}{2}}}, \qquad Z_i = \frac{1}{2\left(\left(\frac{1}{R}\right)^2 + \left(\omega_i C - \frac{1}{\omega_i L}\right)^2\right)^{\frac{1}{2}}}, i = 1, 2 \tag{10}$$

The block diagram of the overall controller with i_{dist} is depicted in Figure 2.

4. Significance of current disturbance injection

The significance of active islanding detection is detailed in this section. The microgrid (comprises equal rated DG and demand) shown in Figure 1 is separated from the grid at time t = 1 s. The response of the frequency at PCC with and without i_{dist} is plotted as shown in Figure 3.

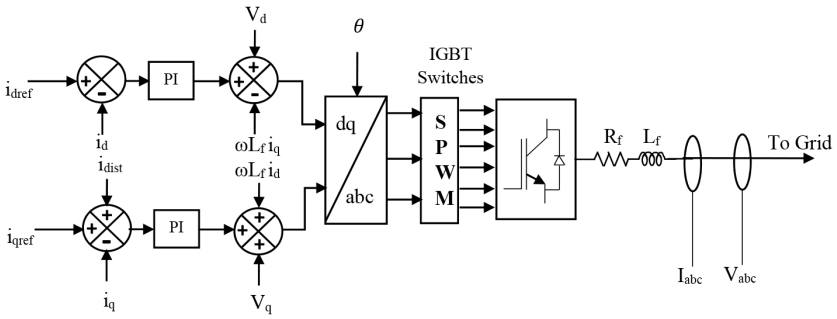

Figure 2. Block diagram of the overall controller with i_{dist}.

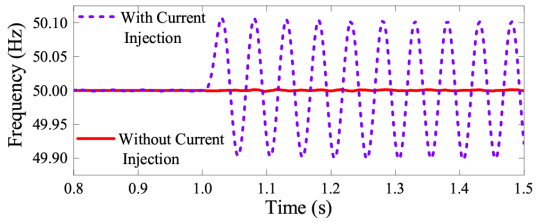

Figure 3. Significance of current disturbance injection.

It is clear from Figure 3 that the variation in frequency is insignificant without i_{dist} on postislanding. The invariant behavior of the frequency possesses a great threat upon failure of most of the earlier devised IDSs. In contrast, with i_{dist}, the frequency varies significantly on postislanding. Hence, the frequency is analyzed further to distinguish between islanding and nonislanding events accurately, as well as to detect islanding faster. Since the current perturbation (intentional disturbance signal is injected through the inverter) is used for islanding detection, it is named active islanding detection.

5. Proposed analyzing methodology

The proposed analysing methodology is expounded in this section. In this work, the current disturbance magnitude of 1% at 20 Hz is chosen [17, 20]. Even though the disturbance signal makes a significant variation on postislanding, an algorithm is essential for an IDS to decide precisely whether the variations occur due to the transients of switching events or islanded state.

In this work, the injection of current disturbance through the q-axis current controller culminates the frequency variation on postislanding due to the nonfundamental frequency components (ω_1 & ω_2), which are forced to flow into the load. The frequency is monitored and the mean of absolute rate of change of frequency is obtained by using the following expression.

5.1. Mean of absolute rate of change of frequency (AROCOFmean)

The rate at which the frequency varies is determined and its mean of the absolute is calculated by the following equation:

$$AROCOFmean(t) = \frac{1}{T}\int_{t-T}^{t} AROCOF(t)\, dt \tag{11}$$

$$AROCOF(t) = |\frac{df}{dt}|, \tag{12}$$

where t is the instantaneous time and T is the time period of the disturbance signal.

The three phase instantaneous voltages at the PCC are measured and the frequency of the same are obtained using the phase locked loop. The deviation in frequency for zero real power mismatched condition on postislanding condition for various quality factors is simulated and the peak deviation values are noted. Based on those values, a generalized expression for the variation in frequency of the voltage signals for various $Q_f s$ are attained through the trendline option in Microsoft Excel and is expressed as follows:

$$Peak\ Frequency\ Deviation = -0.042\ ln(Q_f) + 0.1004 \tag{13}$$

The peak deviations in frequency and ROCOF are depicted in Table 3 for different $Q_f s$ and power ratings.

Table 3. Peak deviation in frequency for 20 Hz of i_{dist} for different $Q_f s$ and DG power ratings.

Q_f	Power rating (MW)	R ($m\Omega$)	L (uH)	C (uF)	Peak deviation in frequency for 20 Hz i_{dist}	Peak deviation ROCOF	Mean of absolute ROCOF
0.5	1	160	1019	9947	0.1293	15.996	10.183
1	1	160	509	19894	0.1007	12.458	7.931
1.8	1	160	283	35810	0.0757	9.365	5.962
2.5	1	160	204	49736	0.0617	7.633	4.859
0.5	5	32	204	49736	0.1293	15.996	10.183
1	5	32	102	99472	0.1007	12.458	7.931
1.8	5	32	57	179050	0.0757	9.365	5.962
2.5	5	32	41	248680	0.0617	7.633	4.859

It is found from Table 3 that for any equally rated generation and demand at a particular Q_f, the peak deviation in frequency is almost the same. The threshold is set to 95% of the absolute mean of ROCOF for safety.

Since the peak deviation in frequency on postislanding remains the same for different DG ratings of any specific quality factor, it is easy to implement the proposed analyzing method without any modification for increased DG power ratings as well as the load.

5.2. Detection signal generation

The three phase instantaneous voltages are measured at the PCC and the frequency signal is obtained using a phase locked loop (PLL). The basic block diagram of the phase locked loop is depicted in Figure 4.

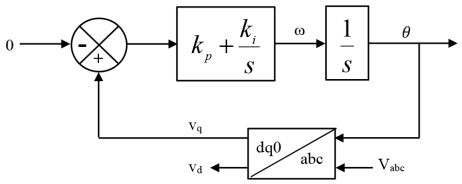

Figure 4. Block diagram of the phase locked loop.

The required θ for abc to dq0 transformation and vice versa is also obtained from the PLL and the

angular frequency corresponding to the dq0 frame is given as follows:

$$\omega = \frac{d\theta}{dt} \tag{14}$$

Subsequently, the ROCOF and AROCOFmean are calculated. The AROCOFmean is compared with the threshold and it is checked if it exceeds the threshold continuously for 80 ms. When the detection signal is set as HIGH, it indicates island formation. The block diagram of the detection signal generation is depicted in Figure 5.

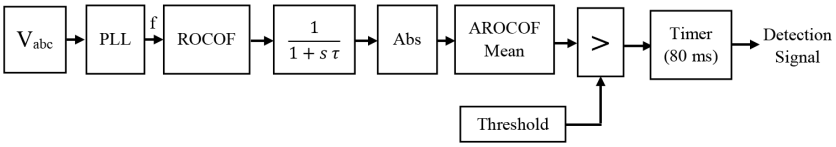

Figure 5. Block diagram of detection signal generation.

As mentioned before, the frequency of the voltage signal is obtained by using the PLL and the derivative of the signal is performed to find the rate of change of frequency (ROCOF). It is passed through the low pass filter (LPF) to attenuate the higher frequency signals in ROCOF and the absolute value is obtained. In order to have a steady (average) signal to be compared with the threshold, the average value of the signal is determined. The AROCOFmean is calculated using Eq. (11) and compared with the threshold. From the block diagram 5, it is observed that if the AROCOFmean exceeds the threshold for a period of 80 ms, the detection signal is set as 'Logical 1' by the timer, indicating an island. If AROCOFmean exceeds the threshold momentarily and does not sustain for 80 ms continuously, it exemplifies a transient condition. Whenever AROCOFmean exceeds threshold the timer gets turned ON and if it falls below the threshold then it will be reset to zero.

The deliberate time delay of 80 ms is chosen, so as to accommodate the extinction of the possible transients as verified in the simulation for different operating conditions. The various international standards have suggested to use a demand Q_f of ≤ 2.5 . As per Table 3, the AROCOFmean of the Q_f 2.5 is less when compared to the other Q_f. In order to decide on a threshold suitable for real time varying demands, the threshold of Q_f 2.5 is used for the validations. It assures that even if the demand varies in real time conditions the threshold need not be adaptive. If an islanding condition occurs for the demand of $Q_f < 2.5$, it is obvious that the variation in frequency would exceed the threshold, since on postislanding the frequency variation for $Q_f < 2.5$ is always more than the frequency variation of $Q_f = 2.5$.

The PAM is depicted as a flowchart in Figure 6. Since the motive behind the present work is to detect island formation, the scope of the detection signal is not discussed any further here.

6. Case studies

The PAM is examined for different working environments comprising islanding events for zero and few power mismatched conditions for different quality factors, and nonislanding events such as grid frequency fluctuations, load switching, and open conductor faults.

The parameters of the test system considered for simulation are mentioned in Table 4.

Table 4. Test system parameters.

Parameter	Value	Parameter		Value	Parameter	Value
R_{fr}	1 $m\Omega$	V_{dc}		0.8 kV	k_{pPLL}, k_{iPLL}	320, 1800
L_{fr}	410 μH	f_{sw}		6000 Hz	τ (LPF)	0.001 s
f_{dist}	20 Hz	Load component	R	160 $m\Omega$	Sample time	2 μs
Load and DG power rating	1 MW		L	204 μH	Current controller parameters (d and q axes)	
Q_f	2.5		C	49.74 mF	k_p	0.8
f_0	50 Hz	V_{rms}		0.4 kV	k_i	200

6.1. Islanding events

6.1.1. Zero power mismatch condition

The PAM is tested for the zero power mismatch condition, since the frequency is hardly influenced without disturbance injection. Where the microgrid (DG with the RLC load) is separated from the grid at 1 s, the generation is considered to match the load exactly. The frequency at PCC, ROCOF, and AROCOFmean for zero power mismatch condition are depicted in Figure 7.

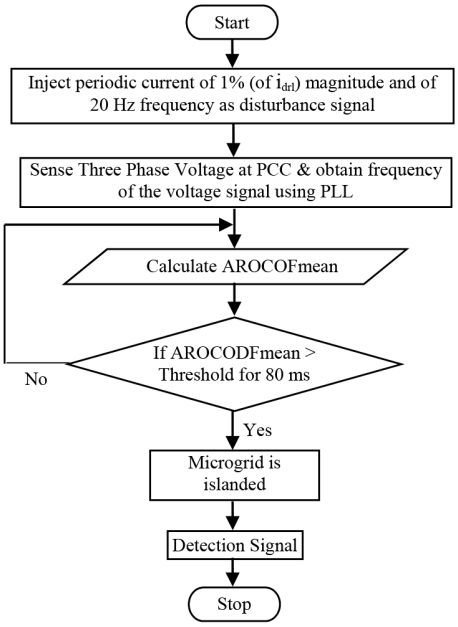

Figure 6. Flowchart of the proposed analyzing method.

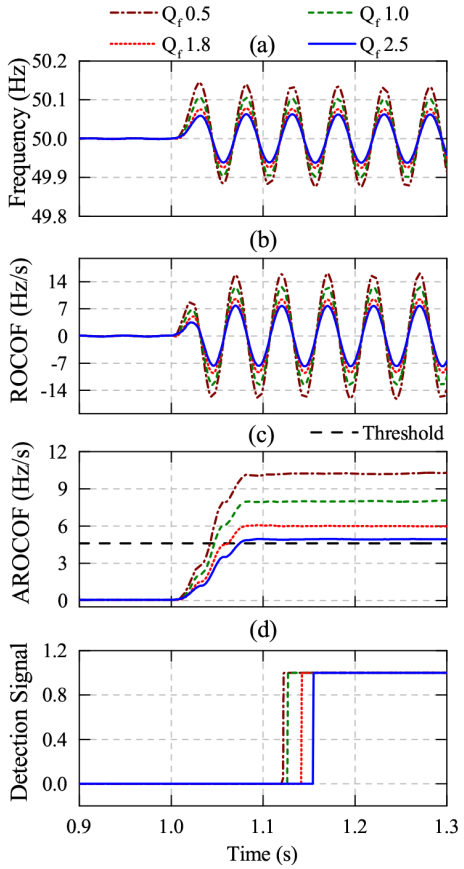

Figure 7. Responses of zero power mismatch situation.

From Figure 7 (c), it is evident that the detection signal is generated within a time period of 160 ms for all the $Q_f s$. The detection time of the PAM is far less than the various islanding standards and also the literature based on the injection of current disturbance in the quadrature axis controller.

6.1.2. Different power mismatch for different quality factors

The IDT for different power mismatch and quality factors is tabulated in Table 5.

Table 5. Detection time of different power mismatch conditions.

Quality factor (Q_f)	Detection time (ms) for power mismatch conditions				
	0%	2.5%	5%	10%	15%
0.5	122.0	120.3	117.9	109.3	103.1
1.0	126.9	122.5	119.2	116.7	127.3
1.8	141.8	132.6	129.3	129.1	126.9
2.5	153.2	152.3	150.4	131.4	128.8

It is found that the detection time is less than the various standards for all quality factors. From table 5, it is clear that the detection time decreases with the decrease in Q_f and also with the increase in power mismatch. The threshold is fixed based on the Q_f 2.5, for the load of $Q_f < 2.5$ AROCODVmean exceeds the threshold faster on postislanding, since the peak deviation in frequency is higher for lower Q_f . Hence, the detection time decreases with the decrease in Q_f. On the other hand, if the power mismatch is more, the momentary variation of frequency is higher at the moment of islanding. Hence, the detection time decreases with the increase in power mismatch. Moreover, the proposed detection method detects island formation faster than the literature [21, 24] based on the disturbance injection in the q-axis current controller, where the detection time is 200 ms for power mismatch of 0%–15%. Furthermore the detection time is found to be less than the few earlier works in the literature as shown in Table 2.

If the real time demand varies, the corresponding Q_f would be less than the Q_f 2.5. Since the threshold is chosen based on the Q_f 2.5, the PAM is most suitable for real time applications (where demand varies continuously) and from Table 5 it is obvious that the detection time will be less for a decrease in Q_f.

6.2. Analysis on NDZ

The nondetection zone is an operating zone where the frequency and voltage are within their operating limits for lower reactive and real power mismatches (between DG generation and the total demand) on postislanding condition, where most of the earlier methods have failed. The PAM is tested for such an operating condition in Section 6.1.1 for the $Q_f s$ of 0.5, 1, 1.8, and 2.5 and also tabulated in Table 5. It is clear from the results that the PAM has zero NDZ.

6.3. Nonislanding events

It is proved that the PAM is capable of detecting island formation faster when compared to the literature based on disturbance injection in the q-axis current controller. However, it is indispensable to validate that the proposed analyzing technique does not malidentify a nonislanded event as island formation. In this section, the proposed analysing method is verified for various nonislanding events.

6.3.1. Grid frequency fluctuations

The grid frequency fluctuates frequently due to various reasons. Here the grid frequency is varied from 50 to 50.5 Hz at 0.6 s and 50.5 to 49.3 Hz at 0.9 s and 49.3 to 50 Hz at 1.2 s, purposely to investigate the significance of the proposed method. The grid frequency is operated to vary within the operating range corresponding to the various standards. The responses of the proposed methodology for the grid frequency fluctuations are shown in Figure 8.

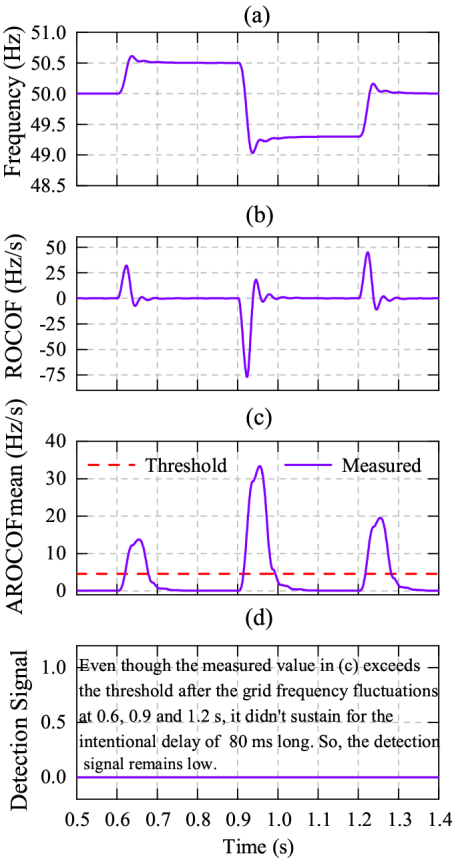

Figure 8. Responses of grid frequency fluctuations.

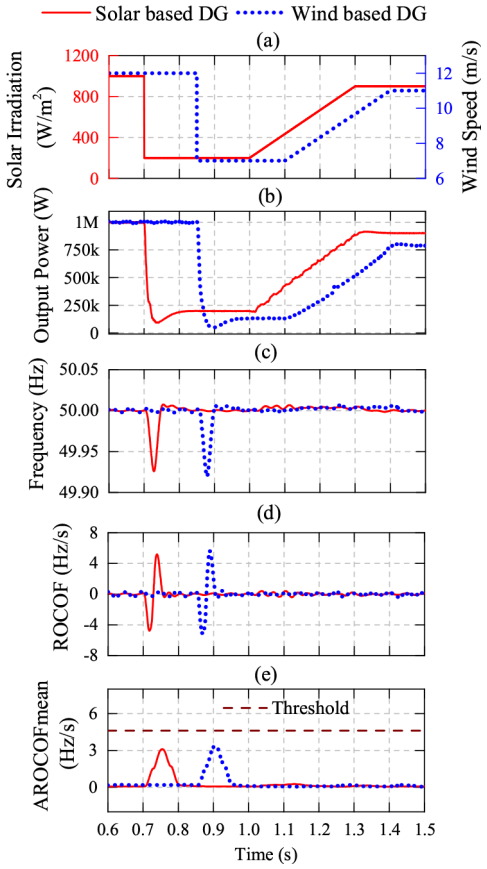

Figure 9. Responses of uncertainities in solar irradiation and wind speed.

In Figure 8 (c), even though the AROCOFmean exceeds the threshold for the grid frequency variations at 0.6, 0.9, and 1.2 s, it does not exceed the threshold for the 80 ms duration. Thus, the grid frequency fluctuations are identified as nonislanding events by the proposed methodology. It is manifested that the proposed methodology is capable of discriminating the islanding condition from the grid-frequency fluctuations very effectively and quickly.

6.3.2. Uncertainties in the solar and wind variations

It is indispensable to validate the PAM for the uncertainties in the solar irradiation and wind velocities as in the real time scenario they are more prone to vary frequently. Instead of solar of 1 MW, a permanent magnet synchronous generator based DG of 1 MW is replaced and it is verified whether the PAM is effective even for wind fluctuations. The reduction in solar irradiation and wind speed leads to reduction in the output power.

To mimic the real time scenario, solar irradiation and wind speed are changed abruptly and linearly and the corresponding results are plotted and analyzed. With the aim of imitating the abrupt and linear change in solar irradiation, the solar irradiation is varied from 1000 to 200 W/m^2 at 0.7 s and 200 to 900 W/m^2 (from 1.0 to 1.3 s) and wind velocity is varied abruptly from 12 m/s to 7 m/s at 0.85s and increases linearly from 7 m/s to 11 m/s between 1.1 and 1.4 s respectively. The results are depicted in Figure 9.

It is apparent from the Figure 9 that the PAM does not consider the transients due to the uncertainties in the solar radiation and wind velocities as an islanded condition. From the results shown in Figure 8 and Figure 9, it is evident that the PAM is capable of differentiating the islanded conditions from other transients.

6.3.3. Different load switching conditions

The distribution system is predominant in load switching (resistive as well as reactive) and hence it is mandatory to validate the proposed methodology for the various load switching instants tested in this section. Mostly the real time loads (which comprise resistive and inductive) are varying in nature. A resistive, inductive, and capacitive load of 1000 kW, 1000 kVAR, and 1000 kVAR are switched IN at 0.7, 1.1, and 1.5 s respectively and switched OUT at 0.9, 1.3, and 1.7 s respectively. The behavior of the various load switchings is pictorially represented in Figure 10.

It is shown in the Figure 10 (c) that the transients due to resistive and inductive load switching do not exceed the threshold for both the switching IN and switching OUT conditions. However, during capacitive load switching the measured value exceeds the threshold but it does not sustain for 80 ms. Therefore, the switching transients due to resistive, inductive, and capacitive load switchings are found as nonislanded events by the proposed methodology without difficulty. Thus, it is discernible that the proposed methodology effortlessly distinguishes this as a nonislanding event.

6.3.4. Open conductor fault

When one or two phases in a circuit breaker open accidentally, the IDS should not malidentify such an operating condition as island formation, since at least one of the three conductors are still closed (remain live). Even though the open conductor fault is not frequent, it is sensible to verify the proposed methodology for such an event. Two phases are made open at 0.7 s to create an open conductor fault and closed at 1.1 s to operate in the normal condition. The responses of the open conductor faults are plotted in Figure 11. The disturbance injected through the two phases of the inverter flows into the load, whereas injected disturbance through the third phase still flows into the grid due to the low impedance path offered by it. Thus, the disturbance injected to the load is not sufficient to make the AROCOFmean exceed the threshold as shown in Figure 11 (c). It is obvious from the results that the proposed method is capable of distinguishing nonislanding events from islanding counterparts effortlessly.

6.3.5. Unbalanced loading condition

The electric distribution system is susceptible to unbalanced loading conditions, and hence it is necessary to verify PAM for the unbalanced loading condition. The three phases of the load (A, B, and C) are initially loaded to their rating. In order to mimic the unbalanced loading condition, the three phases of the load (A, B, and C) are loaded to 50%, 140%, and 75% of their rated values at 0.7, 1.0, and 1.3 s respectively and the responses are depicted in Figure 12.

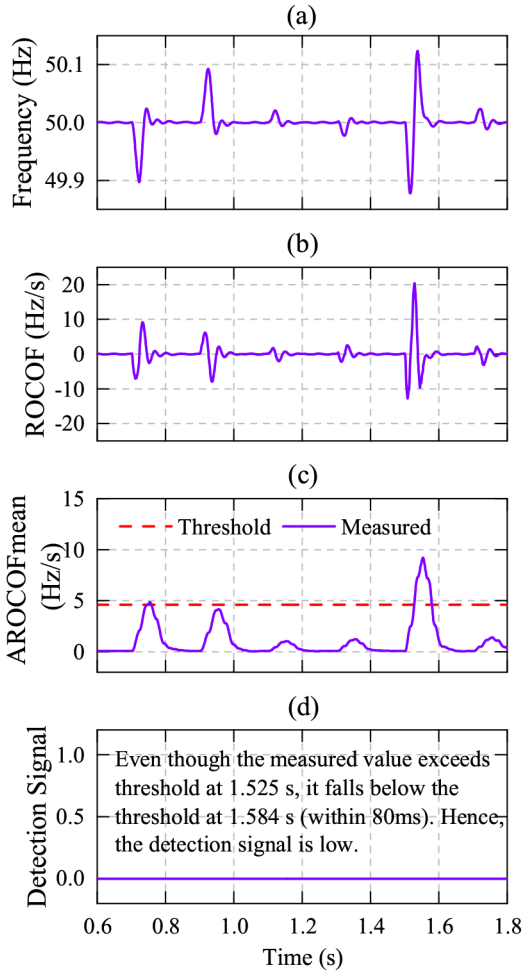

Figure 10. Responses of different load switching conditions.

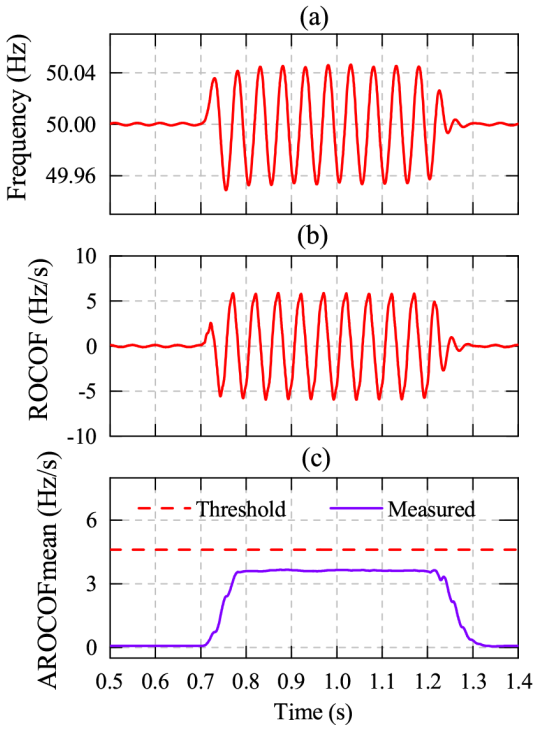

Figure 11. Responses of Open Conductor Fault

It is clear from the responses in Figure 12 that the unbalanced loading condition does not cause significant variation in the frequency of the voltage signal. Hence, the PAM distinguishes this nonislanding event with ease.

6.4. Effect on power quality

It is essential to explain the effect on total harmonic distortion (THD) since the current disturbance injection on the q-axis current controller is given the main focus in this work. The THD of the inverter output current without and with current disturbance injection is plotted in Figure 13.

The THD of the inverter output current is observed to be within the prescribed limit of the IEEE standards [27] for both cases. It is clear from Figure 13 that the THD is increased slightly due to the current disturbance injection through the q-axis current controller. Although there is a slight degradation in power quality, the island formation is detected faster. The grid frequency variation, various switching conditions, and fault conditions are distinguished from the islanded conditions accurately.

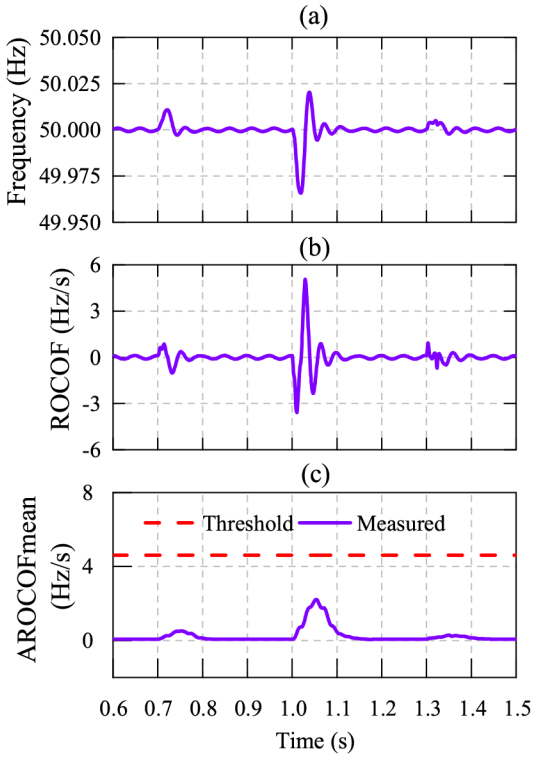

Figure 12. Responses of unbalanced loading conditions.

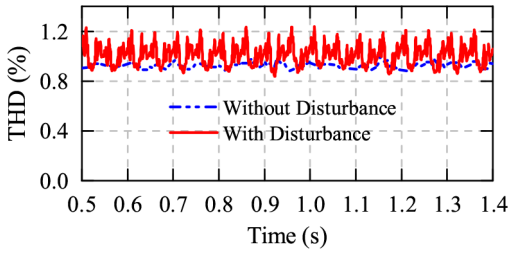

Figure 13. Comparison of the THD of the current components without and with disturbance injection.

6.5. Extendibility for multiple DGs

The proposed analyzing methodology is extendable to multiple inverter based DGs. It is easily applicable to multiple DGs without any modification in intentional delay time, the control circuitry, and also the proposed analyzing method. It is possible to implement the PAM on any inverter based DGs including a permanent magnet synchronous generator with essential converters connected to the microgrid. This is also attempted in this work and the multiple DGs based test system is shown in Figure 14. Each DG is injecting 1% of the rated d-axis current as a disturbance and incorporated with islanding detection scheme it facilitates decentralized islanding detection. Two cases are tested in this section, i.e. Case 1: All 4 DGs are isolated with load from the grid at 0.6 s. Case 2: Only one DG is isolated with load from the rest of the system at 0.6 s. The responses are shown for the zero power mismatch condition in Figure 15.

From Figure 15 it is evident that the control schemes are decoupled and do not disturb the neighboring units in a hybrid system.

7. Conclusion

An active IDS without destabilizing the system based on q-axis current disturbance injection is implemented in this paper. A sinusoidal current disturbance signal of single frequency along with the classical q-axis current signal is injected into the PCC. An analyzing method based on the frequency of the voltage signal is proposed in this work to detect an unplanned island formation. The q-axis current disturbance injection leads to variation in frequency on postislanding, which is evaluated to discriminate islanding and nonislanding events. It is found that the proposed analyzing methodology is capable of detecting islands faster (160 ms), which is considerably less

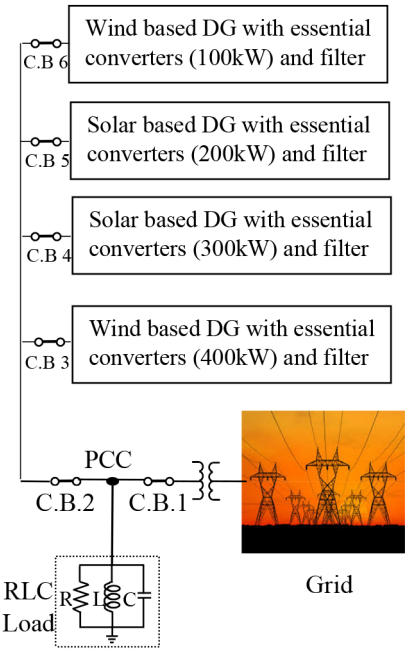

Figure 14. Block diagram of multiple DG system.

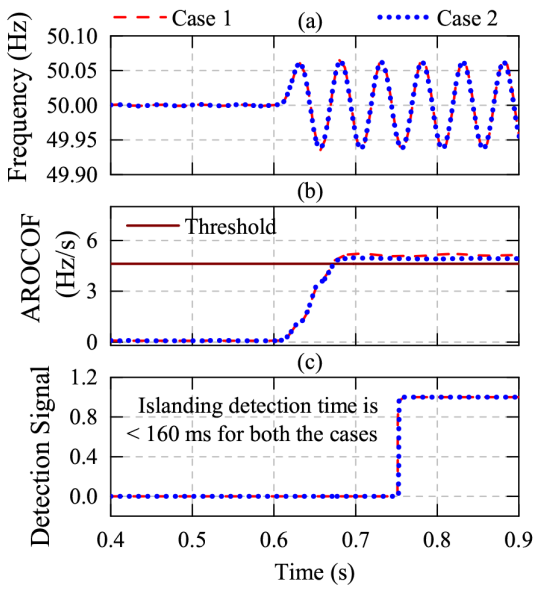

Figure 15. Responses of multiple DGs for zero power mismatch condition.

than the postulated time of various standards. The PAM is also more accurate in discriminating nonislanding instances. The PAM needs no modifications for varying loads for $Q_f < 2.5$, and hence an adaptive threshold is avoided, and thus making the methodology simpler. It is also proved that the PAM is applicable to renewable energy based DG units where the source side fluctuations are also quite common along with grid side fluctuations. The validation of the proposed methodology for multiple DGs has also been presented in this paper with a view to applying the same to a microgrid. The prototype is being developed for the proposed methodology, as a further advancement.

References

[1] Hossain E, Kabalci E, Bayindir R, Perez R. Microgrid testbeds around the world: state of art. Energ Convers Manage 2014; 86: 132-153.

[2] IEEE Recommended practice for utility interface of photovoltaic (PV) systems. IEEE Std 929-2000 2000.

[3] Automatic disconnection device between a generator and the low-voltage grid. DIN-VDE Std 0126; 2005.

[4] Testing procedure of islanding prevention measures for grid connected photovoltaic power generation systems. IEC 62116 2008.

[5] UL standard for safety for inverters, converters, controllers and interconnection system equipment for use with distributed energy resources. UL 1741 2010.

[6] IEEE guide for design, operation, and integration of distributed resource island systems with electric power systems. IEEE Std 1547.4. 2011.

[7] Khamis A, Shareef H, Bizkevelci E, Khatib T. A review of islanding detection techniques for renewable distributed generation systems. Renew Sust Energ Rev 2013; 28: 483-493.

[8] Li C, Cao C, Cao Y, Kuang Y, Zeng L, Fang B. A review of islanding detection methods for microgrid. Renew Sust Energ Rev 2014; 35: 211-220.

[9] Heidari M, Seifossadat G, Razaz M. An intelligence-based islanding detection method using DWT and ANN. Turk J Elect Eng & Comp Sci 2015; 23: 381-394.

[10] Sun R, Centeno VA. Wide area system islanding contingency detecting and warning scheme. IEEE T Power Syst, 2014; 29: 2581-2589.

[11] Bayrak G. A remote islanding detection and control strategy for photovoltaic-based distributed generation systems. Energ Convers Manage 2015; 96: 228-241.

[12] Bayrak G, Kabalci E. Implementation of a new remote islanding detection method for wind – solar hybrid power plants. Renew Sust Energ Rev 2016; 58: 1-15.

[13] Vahedi H, Gharehpetian GB, Karrari M. Application of duffing oscillators for passive islanding detection of inverter based distributed generation units. IEEE T Power Deliver 2012; 27: 1973–1983.

[14] Liu N, Diduch C, Chang L, Su J. A reference impedance based passive islanding detection method for inverter based distributed generation system. IEEE J Em Sel Top P 2015; 3: 1205-1217.

[15] Guha B, Haddad RJ, Kalaani Y. Voltage ripple based passive islanding detection technique for grid connected Photovoltaic Inverters. IEEE Power Energ Technol Syst J 2016; 3: 143-154.

[16] Bakhshi M, Noroozian R, Gharehpetian GB. Novel islanding detection method for multiple DGs based on forced helmholtz Oscillator. IEEE T Smart Grid (in press).

[17] Gonzalez GH, Iravani R. Current injection for active islanding detection of electronically interfaced distributed resources. IEEE T Power Deliver 2006; 21: 1698-1705.

[18] Laghari JA, Mokhlis H, Bakar AHA, Karimi M. A new islanding detection technique for multiple mini hydro based on rate of change of reactive power and load connecting strategy. Energ Convers Manage 2013; 76: 215-224.

[19] Pourbabak H, Kazemi A. A new technique for islanding detection using voltage phase angle of inverter-based DGs. Int J Elec Power 2014; 57: 198–205.

[20] Gupta P, Bhatia RS, Jain DK. Average absolute frequency deviation value based active islanding detection technique. IEEE T Smart Grid 2015; 6: 26-35.

[21] Emadi A, Afrakhte H. A reference current perturbation method for islanding detection of a multi-inverter system. Electr Pow Syst Res 2016; 132: 47-55.

[22] Chen X, Li Y. An islanding detection method for inverter-based distributed generators based on the reactive power disturbance. IEEE T Power Electr 2016; 31: 3559-3574.

[23] Liu S, Zhuang S, Xu Q, Xiao J. Improved voltage shift islanding detection method for multi-inverter grid-connected photovoltaic systems. IET Gener Transm Dis 2016; 10: 3163-3169.

[24] Gupta P, Bhatia RS, Jain DK. Active ROCOF relay for islanding detection. IEEE T Power Deliver 2017; 32: 420-429.

[25] Murugesan S, Murali V, Daniel SA. Hybrid analyzing technique for active islanding detection based on d-axis current injection. IEEE Syst J (in press).

[26] Bei TZ. Accurate active islanding detection method for grid-tied inverters in distributed generation. IET Renew Power Gen 2017; 11: 1633-1639.

[27] IEEE recommended practice and requirements for harmonic control in electric power systems - redline. IEEE Std 519-2014 (Revision of IEEE Std 519-1992) - Redline 2014: 1-213.